Raman scattering from superlattices of diluted magnetic semiconductors

E.-K. Suh, D. U. Bartholomew, A. K. Ramdas, and S. Rodriguez
Department of Physics, Purdue University, West Lafayette, Indiana 47907

S. Venugopalan
Department of Physics, State University of New York, Binghamton, New York 13901

L. A. Kolodziejski and R. L. Gunshor
School of Electrical Engineering, Purdue University, West Lafayette, Indiana 47907
(Received 6 March 1987)

Collective and localized excitations in superlattices of the Mn-based II-VI diluted magnetic semiconductors $Cd_{1-x}Mn_xTe/Cd_{1-y}Mn_yTe$ and $ZnSe/Zn_{1-x}Mn_xSe$ have been investigated with use of Raman scattering. The new periodicity introduced by the superlattice causes zone folding of the acoustic phonons allowing modes with large q vectors, normally inactive in light scattering, to become Raman active; their frequencies can be understood in terms of the elastic constants of the two constituents. In the optical-phonon region, the Raman spectra of the superlattices with superlattice axis along [001] show optical phonons "confined" to the well or the barrier layer when the corresponding dispersion curves do not overlap, whereas "propagating" optical phonons are observed when they do. In [111] $Cd_{1-x}Mn_xTe/Cd_{1-y}Mn_yTe$ superlattices, interface optical phonons are selectively favored in Raman scattering by the intermediate states associated with excitons localized at the heterointerfaces. In $ZnSe/Zn_{1-x}Mn_xSe$ superlattices, the strain arising from lattice mismatch gives rise to shifts in the optical-phonon frequencies. The large magnetic field shifts in the photoluminescence associated with the electronic transitions in the well demonstrate the existence of large exchange interaction between the band electrons and Mn^{2+}, as in bulk crystals. This effect can be exploited in the magnetically tuned resonance enhancement of the Raman spectrum of optical phonons. In the presence of an external magnetic field, as in the bulk, Raman electron paramagnetic resonance of Mn^{2+} is observed. The absence of a magnon feature is indicative of the absence of magnetic ordering in superlattices. In the [111] $Cd_{1-x}Mn_xTe/Cd_{1-y}Mn_yTe$ superlattice, a new Raman line is observed which can be interpreted as a transition in the isolated Mn^{2+} pairs; its position yields a value of the nearest-neighbor exchange interaction $|J_{NN}|=(6.8\pm0.2\ \mathrm{K})k_B$.

I. INTRODUCTION

Semiconductor superlattices are of great interest because of their unique physical properties and potential for device applications. These two-dimensional structures are grown by either molecular-beam epitaxy (MBE) or metalorganic chemical-vapor deposition (MOCVD). The most extensively studied superlattices have been those composed of III-V compounds such as GaAs/$Ga_{1-x}Al_xAs$. Recently, multiple quantum wells and superlattices containing diluted magnetic semiconductors (DMS's) have been grown successfully by MBE.[1-3]

A DMS is a II-VI semiconducting compound which contains magnetic ions, such as Mn^{2+}, at random locations on the group-II sublattice, e.g., $Cd_{1-x}Mn_xTe$. These alloys occur in a homogeneous crystalline phase with either the zinc-blende or the wurtzite structure over a large composition range. As semiconducting alloys, DMS's display important composition-dependent behavior such as the dependence of the band gap (E_g) and lattice parameter (a) on the Mn^{2+} concentration (x). Furthermore, the presence of the magnetic ions endows unique properties to DMS's and their superlattices.[4] For example, these alloys display magnetic phase transitions and magnetic excitations. Also, the spin-spin exchange interaction between the magnetic moments of the localized Mn^{2+} ions and those of the band electrons (the sp-d exchange interaction) leads to a dramatic enhancement of the Zeeman splitting of electronic energy levels comparable to minigaps and other energy parameters.

As a bulk crystal, $Cd_{1-x}Mn_xTe$ occurs in the zinc-blende structure for $0\le x\le 0.7$, while $Zn_{1-x}Mn_xSe$ has the zinc-blende structure for $0\le x\le 0.30$ and the wurtzite structure for $0.33\le x\le 0.57$.[5] However, $ZnSe/Zn_{1-x}Mn_xSe$ superlattices of the cubic zinc-blende phase have been grown successfully by MBE for the entire composition range.[6] The lattice parameter in these materials changes linearly with x resulting in a lattice mismatch at the interfaces. The lattice mismatch is accommodated by a homogeneous strain in the layers resuling in a "strained layer superlattice" (SLS). Such a strain can be particularly large in the $Zn_{1-x}Mn_xSe/Zn_{1-y}Mn_ySe$ superlattices.

In this paper, we report an investigation of the DMS superlattices $Cd_{1-x}Mn_xTe/Cd_{1-y}Mn_yTe$ and $Zn_{1-x}Mn_xSe/Zn_{1-y}Mn_ySe$ using Raman scattering.

II. EXPERIMENTAL PROCEDURE

We have investigated $Cd_{1-x}Mn_xTe/Cd_{1-y}Mn_yTe$ superlattices with the axis normal to the layer planes—the

TABLE I. Parameters of samples.

Sample	Well	Barrier	d_1 (Å)	d_2 (Å)	Number of periods (n)	Orientation	Buffer layer
SL-4	$Cd_{0.89}Mn_{0.11}Te$	$Cd_{0.50}Mn_{0.50}Te$	59	59	135	[111]	$Cd_{0.50}Mn_{0.50}Te$
SL-8	CdTe	$Cd_{0.76}Mn_{0.24}Te$	71	128	128	[111]	$Cd_{0.70}Mn_{0.30}Te$
SL-9	CdTe	$Cd_{0.70}Mn_{0.30}Te$	650	650	61	[111]	$Cd_{0.70}Mn_{0.30}Te$
SSL-2	CdTe	$Cd_{0.75}Mn_{0.25}Te$	57	96	30	[001]	CdTe & $Cd_{0.75}Mn_{0.25}Te$
SSL-3	CdTe	$Cd_{0.75}Mn_{0.25}Te$	84	94	20	[001]	CdTe & $Cd_{0.75}Mn_{0.25}Te$
ZSL-2	ZnSe	$Zn_{0.77}Mn_{0.23}Se$	63	104	67	[001]	ZnSe
ZSL-3	ZnSe	$Zn_{0.67}Mn_{0.33}Se$	97	175	67	[001]	ZnSe
ZSL-4	ZnSe	$Zn_{0.49}Mn_{0.51}Se$	73	180	67	[001]	ZnSe
ZSL-11	ZnSe	$Zn_{0.74}Mn_{0.26}Se$	24	160	76	[001]	ZnSe & $Zn_{0.74}Mn_{0.26}Se$
ZSL-12	ZnSe	$Zn_{0.67}Mn_{0.33}Se$	29	170	76	[001]	ZnSe & $Zn_{0.67}Mn_{0.33}Se$

superlattice axis—along [001] or [111] as well as $ZnSe/Zn_{1-x}Mn_xSe$ superlattices with their superlattice axis along [001]; the samples are grown on (001) surfaces of GaAs substrate followed by $Cd_{1-x}Mn_xTe$ or $Zn_{1-x}Mn_xSe$ buffer layers. Various parameters characterizing the different samples are listed in Table I. Details of their fabrication are described elsewhere.[1,2,7] Transmission electron microscopy shows that these superlattices have sharp interfaces separating the successive layers.[2,8]

Raman spectra were obtained in the backscattering geometry using several discrete lines provided by a Kr^+ laser, He-Ne laser, and an Ar^+ laser, as well as radiation from a tunable ring dye laser operating with the compound 4-dicyanomethylene-2-methyl-6-*p*-dimethylaminostyryl-4*H*-pyran (DCM). The incident laser beam is passed through a polarization rotator to achieve the desired incident polarization and is focused onto the sample using either cylindrical or spherical lenses. Typical laser power (P_L) ranged from 50 to 100 mW. The scattered radiation was analyzed with a computer-controlled double (triple) monochromator and detected with standard photon-counting electronics. The polarization of the scattered radiation was analyzed using a linear polarizer.

Low-temperature measurements were performed with either a glass cryostat or a variable-temperature stainless-steel cryostat. Magnetic-field-dependent measurements were carried out with a variable-temperature optical cryostat equipped with a superconducting coil providing external magnetic fields up to 60 kG.

III. RESULTS AND DISCUSSIONS

A. Folded acoustic phonons

Figure 1 shows the low-frequency Raman spectra for [111] $Cd_{1-x}Mn_xTe/Cd_{1-y}Mn_yTe$ superlattices excited with the 6764-Å line of a Kr^+ laser at room temperature. All the spectra were recorded in the $z'(x'x')\bar{z}'$ scattering configuration: here x' and y' are in the plane of the layers with z' along the superlattice axis. The incident laser radiation has an energy $\hbar\omega_L$ intermediate between the band gap of the well and that of the barrier layers. Bulk crystals corresponding to the constituent materials of the superlattices show no Raman lines due to phonons in this spectral region. We attribute these lines to the longitudinal acoustic (LA) phonons folded into the new Brillouin zone, which arises from the additional periodicity of the superlattice. Raman scattering from folded LA phonons has been reported previously for $GaAs/Ga_{1-x}Al_xAs$,[9,10,11] Si/Si_xGe_{1-x},[12] and amorphous Si/SiN_x (Ref. 13) superlattices, as well as in a $Cd_{0.89}Mn_{0.11}Te/Cd_{0.50}Mn_{0.50}Te$ (Ref. 14) superlattice.

Since the acoustic dispersion curves of the two constitutent materials of the superlattice overlap over a wide frequency range, acoustic phonons can propagate through both layers. For long-wavelength acoustic phonons one can apply a model in which the superlattice is considered as an elastic continuum composed of two alternating layers characterized by densities ρ_1 and ρ_2, and by bulk longitudinal acoustic velocities v_1 and v_2 along the superlattice axis.[9] The dispersion relation for the acoustic phonons propagating along the superlattice axis with wave vector q_z is given by[15]

$$\cos(q_z D)=\cos\left[\frac{\omega d_1}{v_1}\right]\cos\left[\frac{\omega d_2}{v_2}\right] -(1+\delta)\sin\left[\frac{\omega d_1}{v_1}\right]\sin\left[\frac{\omega d_2}{v_2}\right], \quad (1)$$

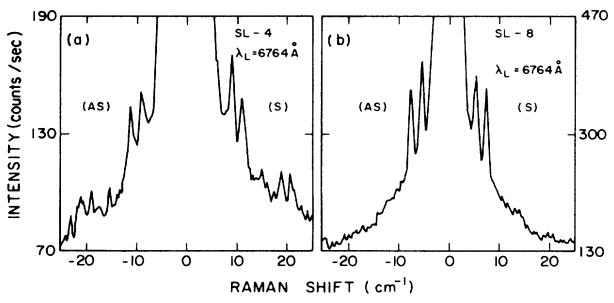

FIG. 1. Stokes (S) and anti-Stokes (AS) components of the folded longitudinal acoustic phonons in $Cd_{1-x}Mn_xTe/Cd_{1-y}Mn_yTe$ superlattices with $\hat{z}'\|[111]$; (a) SL-4, $P_L=120$ mW, and (b) SL-8, $P_L=100$ mW. See Table I for parameters.

where d_1 and d_2 are the respective thicknesses of the well and barrier layers, $D=d_1+d_2$, and $\delta=\frac{1}{2}(\rho_1 v_1-\rho_2 v_2)^2/(\rho_1 v_1 \rho_2 v_2)$. From Eq. (1) one can deduce that the dispersion curve of the average bulk material is folded into the new Brillouin zone; in addition, small gaps open up at the zone center and the boundary when δ is different from zero. As a result of this zone folding, additional "zone-center" modes which can interact with the electromagnetic radiation can be observed in Raman scattering.

In Fig. 2, folded LA phonons in [001] $Cd_{1-x}Mn_xTe/Cd_{1-y}Mn_yTe$ and [001] $ZnSe/Zn_{1-x}Mn_xSe$ superlattices are shown. Figure 2(b) shows the second and third doublets of folded LA phonons in ZSL-4, excited with the 4765-Å line of the Ar^+ laser; the higher-frequency peak of the first doublet is also observed when a finer resolution is used. Using the interpolated values of the densities and elastic moduli for various compositions of bulk $Cd_{1-x}Mn_xTe$ (Refs. 16 and 17) and $Zn_{1-x}Mn_xSe$,[18] one can calculate the frequencies of LA phonons as a function of the wave vector $\mathbf{q}$. In the backscattering geometry, the wave vector of the scattered radiation is $q_s=2(2\pi n/\lambda_L)$, where n is the refractive index of the sample. The longitudinal sound velocity along the [001] direction is given by $(c_{11}/\rho)^{1/2}$ and along the [111] direction by $[\frac{1}{3}(c_{11}+2c_{12}+4c_{44})/\rho]^{1/2}$. For example, in the [111] $Cd_{0.89}Mn_{0.11}Te/Cd_{0.50}Mn_{0.50}Te$ superlattice, SL-4, the densities[17] and the sound velocities[17] are given by

$$\rho_1=5.745\ \text{g/cm}^3,\quad v_1=3.447\times10^5\ \text{cm/sec};$$

$$\rho_2=5.330\ \text{g/cm}^3,\quad v_2=3.482\times10^5\ \text{cm/sec}.$$

The solutions of Eq. (1) with these parameters are 8.8 and 10.8 cm^{-1} for the first doublet and 18.6 and 20.5 cm^{-1} for the second doublet, in an excellent agreement with the experimental values of 9.2, 11.0, 19.0, and 20.7 cm^{-1}, respectively. The strain associated with the lattice mismatch between the alternate layers is estimated to be less than ±0.007 in both layers. With the Grüneisen constant estimated from the pressure derivative of the bulk elastic constants,[19] ranging from 1.0 to 1.3 for $Cd_{1-x}Mn_xTe$ ($x=0$ to $x=0.5$), the change in the frequencies of LA phonons due to strain are expected to be insignificant in the context of the present measurements. The calculated frequencies of folded LA phonons for various superlattices are marked on the dispersion curves of each sample in Fig. 3. The measured frequencies of the folded LA phonons in the [111] $CdTe/Cd_{1-x}Mn_xTe$ superlattice, SL-8, are in a reasonable agreement with the calculated values, as can be seen in Fig. 3(a). Figure 3(c) also shows an excellent agreement up to the third-order doublet in the $ZnSe/Zn_{1-x}Mn_xSe$ superlattice, ZSL-4. However, in the [001] $CdTe/Cd_{1-x}Mn_xTe$, SSL-2, the deviation of the measured values from the calculated values is significant as can be seen in Fig. 3(b). Since the strain associated with the lattice mismatch cannot be invoked to explain this discrepancy, we speculate that it may be a consequence of the small number of periods, $n=30$, for this particular sample.

Finally, we note that the intensities of folded LA phonons are extremely weak in the $ZnSe/Zn_{1-x}Mn_xSe$ superlattices, ZSL-11 and ZSL-12, which have very thin well layers as compared to the thicknesses of the barrier layers. The Raman intensity of the folded LA phonons can be described by a photoelastic mechanism.[20] The intensity of the Raman line corresponding to the mth-order folded LA phonons is proportional to $(1/m^2)\sin^2(m\pi d_1/D)$. Thus the intensity of the first doublet is a maximum when d_1 and d_2 are equal and decreases as the ratio d_1/D decreases. On the other hand, the intensity of the second doublet is zero for the superlattices with $d_1=d_2$, and is still negligible if d_1/D is very small. However, the second doublet is indeed observed under the resonance conditions in SL-4, which has $d_1=d_2$, as shown in Fig. 1(a).

B. Confined, propagating, and interface optical phonons

In this section we focus on Raman scattering from vibrational excitations in DMS superlattices with frequencies comparable to those of optical phonons in the bulk DMS's. In this context it is useful to recall some of the relevant features of the optical phonons in the bulk and their modifications expected in a superlattice.

Due to the significant difference in the masses of Cd and Mn, $Cd_{1-x}Mn_xTe$ exhibits a "two-mode" behavior having two pairs of lines characteristic of zone-center "CdTe-like" and "MnTe-like" LO-TO phonons.[21] The

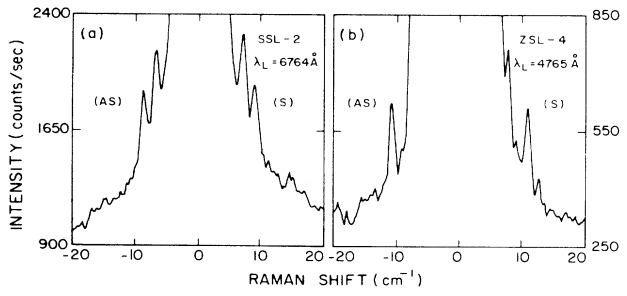

FIG. 2. Folded longitudinal acoustic phonons in CdTe/$Cd_{0.75}Mn_{0.25}Te$ and $ZnSe/Zn_{0.67}Mn_{0.33}Se$ superlattices with $\hat{\mathbf{z}}\|[001]$; (a) SSL-2 and (b) ZSL-4. See Table I for parameters.

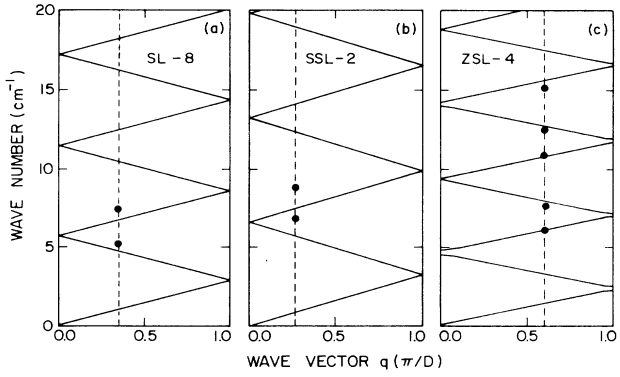

FIG. 3. Dispersion curves for the folded LA phonons calculated using the elastic continuum theory. Observed Raman shifts are shown with dots, the size of dots being indicative of the error bars; (a) SL-8, (b) SSL-2, and (c) ZSL-4.

localized mode of Mn impurity in CdTe evolves into the LO and TO modes of hypothetical zinc-blende "MnTe" while the LO and TO modes of "CdTe" merge into the gap mode of Cd in "MnTe." The behavior of optical phonons in this alloy system has been interpreted by Peterson *et al.*[22] using a modified random element isodisplacement model. In contrast, optical phonons in $Zn_{1-x}Mn_xSe$ (Ref. 23) exhibit a mixed-mode behavior intermediate between "two-mode" and "one mode" as in $Zn_{1-x}Mn_xTe$:[22] the LO phonon of ZnSe continuously evolves into that of MnSe (LO_1) while the TO phonon (TO_2) and one of the components of the Mn^{2+} impurity mode in ZnSe (LO_2) merge into the gap mode of Zn in the hypothetical zinc-blende "MnSe." The other Mn^{2+} impurity component (TO_1) transforms into the TO phonon of "MnSe."

We now discuss the difference between the vibrational excitations for bulk crystals and those for the superlattices in the context of the matching of the optical-phonon frequencies in the two constituent layers. The dispersion curves for LO phonons in bulk CdTe and $Cd_{1-x}Mn_xTe$ ($x=0.25$) calculated using the linear chain model with nearest-neighbor interaction only and assuming that Mn^{2+} ions randomly replace the Cd^{2+} ions in the mixed crystal $Cd_{1-x}Mn_xTe$ are shown in Fig. 4. This plot indicates that in $CdTe/Cd_{1-x}Mn_xTe$ superlattices, the MnTe-like phonon mode of the $Cd_{1-x}Mn_xTe$ layers cannot propagate into the CdTe layers because of the large attenuation of the vibration in that frequency region (region I). Similarly, in the frequency region between the CdTe zone-center LO phonon and the CdTe-like zone-center LO phonon of the $Cd_{1-x}Mn_xTe$ layer (region II), the CdTe LO mode cannot be sustained in the $Cd_{1-x}Mn_xTe$ layers. Therefore, these phonon modes can be considered to be confined to their respective layers, resulting in quantized optical phonons which are equivalent

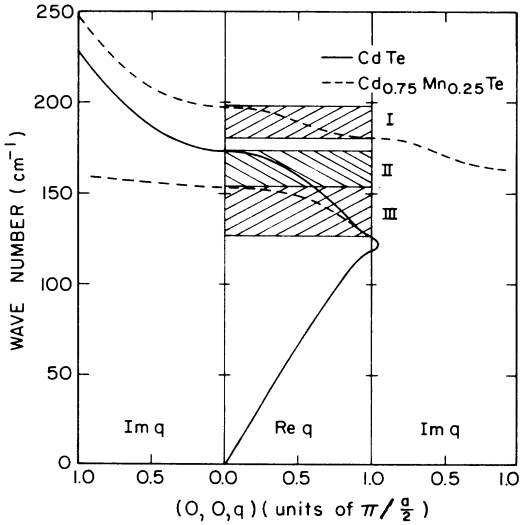

FIG. 4. Dispersion curves of LO phonons in bulk CdTe and in $Cd_{0.75}Mn_{0.25}Te$ calculated using the linear chain model. Solid curve, CdTe; dashed curves, $Cd_{0.75}Mn_{0.25}Te$. I and II are frequency ranges of confined optical phonons whereas III corresponds to propagating optical phonons.

to vibrations in the bulk material whose wave vectors are given by[24] $q=m\pi/(d+a/2)$, where $d=d_1$ or d_2, the thickness of the CdTe (1) or the $Cd_{1-x}Mn_xTe$ (2) layer, and m is an integer. On the other hand, in the frequency region of CdTe-like phonon modes in the $Cd_{1-x}Mn_xTe$ layers (region III), the vibrations of $Cd_{1-x}Mn_xTe$ layers and CdTe layers can propagate into both layers: the coupling between excitations originating in different layers may result in an average collective excitation[25] as in the case of the acoustical phonons discussed in Sec. III A.

We note that, as in the bulk crystal, in a superlattice one can obtain a selective enhancement of the intensities of the Raman lines associated with optical phonons from the well or the barrier layers by matching either the incident or the scattered photon energy with electronic transitions;[26,27] in superlattices the relevant electronic transitions can be associated with either the well or the barrier.

For finite crystals like thin films, or layers in superlattices and heterostructures, the existence of surfaces or interfaces results in new vibrational excitations in addition to the "bulk" vibrational excitations which we discussed earlier. These additional vibrational modes are the surface modes in thin ionic slabs[28] or the "interface" vibrational (IF) modes in superlattices. IF modes have recently been observed by Raman scattering[29,30] as well as by high-resolution electron-energy-loss spectroscopy[31] (HREELS) in $GaAs/Ga_{1-x}Al_xAs$ superlattices. IF modes propagate along the interface planes and are highly localized near them; the amplitude of an IF mode decays exponentially in the direction perpendicular to the layer plane. One of the characteristics of IF modes is that their Raman intensity is resonantly enhanced when the incident photon energy is close to the electronic transitions of either the well or barrier layer since its vibrational amplitude does not vanish in either layer. In addition, the frequencies of IF modes observed in Raman scattering greatly depend on the incident photon energy. These characteristics distinguish Raman lines which are associated with IF modes.

Another consequence of the formation of the superlattice is the strain due to the lattice mismatch between two constituent layers. The lattice parameter in bulk DMS crystals changes almost linearly with the manganese concentration. For example, the lattice parameter of bulk $Cd_{1-x}Mn_xTe$ is given by $a=6.487-0.149x$ Å,[32] whereas that of bulk (or epitaxial film) $Zn_{1-x}Mn_xSe$ shows a stronger dependence on x, viz., $a=5.666+0.268x$ Å.[33] Therefore, the lattice mismatch in $ZnSe/Zn_{1-x}Mn_xSe$ superlattices is significantly larger and the shift of the optical-phonon frequencies due to such large strains must be considered; further discussions are given in Sec. III B 3. On the other hand, such strains in most of the $Cd_{1-x}Mn_xTe/Cd_{1-y}Mn_yTe$ superlattices are not significant and do not appear to be important in the interpretation of their Raman spectra.

1. [001] $Cd_{1-x}Mn_xTe/Cd_{1-y}Mn_yTe$ superlattices

Figure 5 shows the Raman spectra of a [001] $CdTe/Cd_{0.75}Mn_{0.25}Te$ superlattice (SSL-2) at $T=80$ K in the frequency region of optical phonons with various wavelengths of laser excitation (λ_L). In Fig. 5(a), ob-

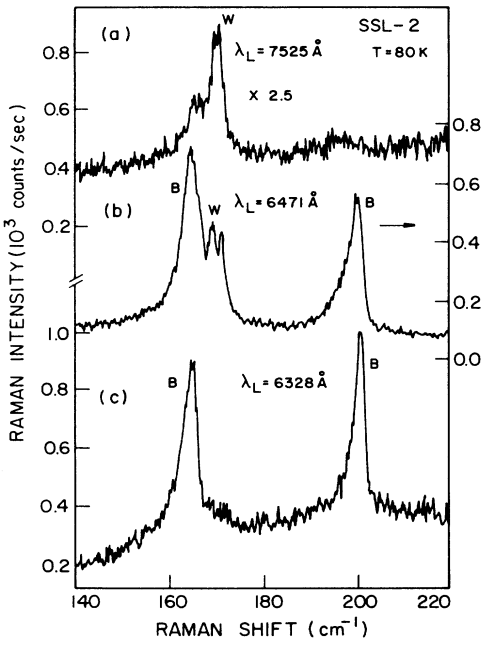

FIG. 5. Raman spectra from optical phonons in [001] $CdTe/Cd_{0.75}Mn_{0.25}Te$ obtained at $T=80$ K. Spectra were excited with three different laser wavelengths: (a) $\lambda_L=7525$ Å, (b) $\lambda_L=6471$ Å, and (c) $\lambda_L=6328$ Å; $P_L=50$ mW. Phonons originating from the CdTe well layers and the $Cd_{0.75}Mn_{0.25}Te$ barrier layers are labeled *W* and *B*, respectively.

tained with $\lambda_L=7525$ Å, i.e., with photon energy ($\hbar\omega_L$) close to the lowest electronic transition of the CdTe well, the LO phonon of CdTe appears resonantly enhanced whereas those of the $Cd_{0.75}Mn_{0.25}Te$ barrier are weak. As the incident photon energy is increased to a value lying between the energy gaps of the two layers, LO phonons from the CdTe well as well as those from the $Cd_{0.75}Mn_{0.25}Te$ barrier are observed as shown in Fig. 5(b). When the incident photon energy approaches the bandgap of $Cd_{0.75}Mn_{0.25}Te$, only the phonons from the barrier layer are observed as shown in Fig. 5(c). These spectra illustrate the resonance enhancement of intensities of phonons associated with the different layers as discussed earlier. By choosing the appropriate incident photon energy, we can thus obtain a selective resonance enhancement of the LO phonons in either superlattice layer.

In Fig. 6, we show once more the Raman spectrum of SSL-2, recorded at $T=80$ K. The peak at ~ 200 cm^{-1} is the MnTe-like LO phonon from the barrier layer. The peaks between 160 and 173 cm^{-1} are due to the CdTe-like and CdTe LO phonons of the barrier and well layers, respectively. The frequencies and shapes of these Raman lines are different from the LO phonons seen in the bulk crystals. The most prominent peak at 165 cm^{-1} is the CdTe-like LO phonon of $Cd_{0.75}Mn_{0.25}Te$, which propagates through both layers. Although this mode is expected to be folded, the Raman line does not resolve into multiple peaks since the frequencies of this mode do not change substantially with the variation of the wave vector. The peaks labeled $n=2$, 4, and 6 are

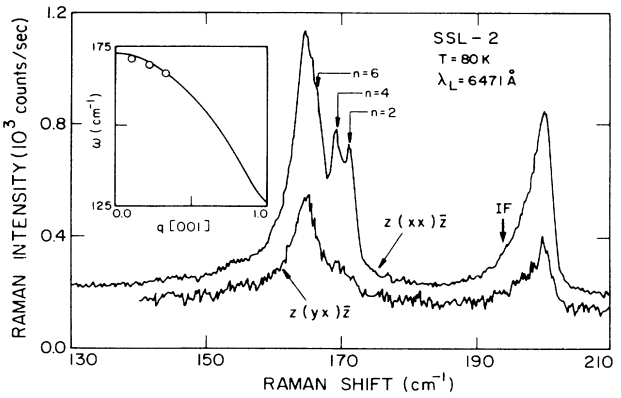

FIG. 6. Raman spectra from optical phonons in a [001] $CdTe/Cd_{0.75}Mn_{0.25}Te$ superlattice for different polarizations. Confined optical phonons are labeled with $n=2$, 4, and 6. Inset shows the observed frequencies of the confined LO phonons plotted on the bulk CdTe dispersion curve calculated with a linear chain model.

attributed to the LO phonons confined to the CdTe layers.

In the [001] superlattice, belonging to the point group D_{2d}, the phonons observed in Raman scattering have symmetry A_1 for $z(xx)\bar{z}$ scattering and B_2 for $z(xy)\bar{z}$ scattering.[34] Here x,y,z are along the cubic axes, z being the superlattice axis. A_1 phonons, which dominate the Raman spectra of the well under resonance condition, have wave vectors characterized by even m values, while B_2 phonons, which can be observed far from resonance, have wave vectors with odd m values.[35] In Fig. 6, the confined LO phonons of the CdTe layers appear in the (xx) polarization and hence these phonons should be assigned to the even m values, 2, 4, and 6. Their frequencies are given by $\omega(q_m)$, where $\omega(\mathbf{q})$ is the dispersion of the LO phonon in bulk CdTe and $q_m=m\pi/(d_1+a/2)$. With this assignment, their measured frequencies are in excellent agreement with the dispersion curve calculated by the linear chain model for CdTe as shown in the inset in Fig. 6. Although not resolved into the additional peaks due to the absence of significant variation of frequency with wave vector and the large layer thickness, the peak at the MnTe-like LO mode of the $Cd_{1-x}Mn_xTe$ layer has a frequency shifted to the lower energy due to the confinement effect.[36] Furthermore, this peak shows a marked low-energy asymmetry which resolves into a weak additional peak labeled "IF" at the low-energy side when the incident photon energy approaches the electronic subband transitions of the well layer. This additional peak is even better resolved in the overtone region as shown in Fig. 7. A similar peak is observed in SSL-3, whose Raman spectra are shown in Fig. 8. With $\lambda_L=6471$ Å, the Raman lines due to LO phonons from the well as well as barrier layers appear in the spectrum. In this superlattice the confined LO phonons of the CdTe layer are not resolved due to the large well thickness. One can also notice the low-energy asymmetry of MnTe-like LO phonon. When the incident photon resonants with the CdTe well transitions, both CdTe-like and MnTe-like LO phonons of $Cd_{0.75}Mn_{0.25}Te$ barrier layer become very weak, while the

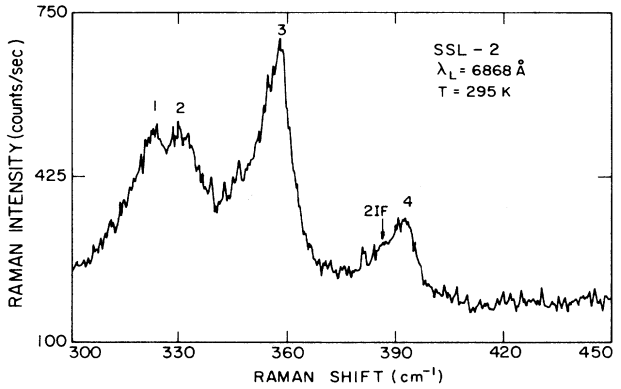

FIG. 7. Overtones and combinations of LO phonons in SSL-2. The line labels denote the following assignments: (1) $2LO_{B,1}$, (2) $2LO_W$, (3) $LO_{B,1} + LO_{B,2}$, and (4) $2LO_{B,2}$, where the subscripts W and B represent the well and barrier layers, respectively, and 1 and 2 represent the CdTe-like and MnTe-like phonons, respectively. 2IF is the overtone of the MnTe-like interface mode which causes the low-frequency asymmetry of the MnTe-like LO phonon in Fig. 6.

peak located between the MnTe-like LO and TO phonons labeled "IF" as well as the CdTe LO phonon appear strongly, as can be seen in Fig. 8(b). The peak labeled "IF" is attributed to an interface mode; we will defer the basis for this assignment to the discussion of the results obtained with [111] superlattices. In summary, for the [001] superlattices we have identified LO phonons confined to the well or barrier layers as well as LO phonons propagating through both layers.

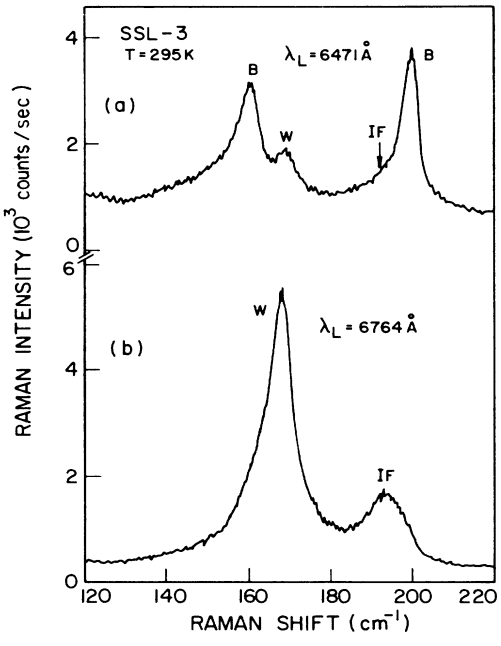

FIG. 8. Raman scattering from LO phonons in the [001] $CdTe/Cd_{0.75}Mn_{0.25}Te$ superlattice, SSL-3, excited with (a) $\lambda_L = 6471$ Å, (b) $\lambda_L = 6764$ Å. W and B represent the phonons originating from well and barrier layers, respectively. IF represents the interface phonon.

2. *[111] $Cd_{1-x}Mn_xTe/Cd_{1-y}Mn_yTe$ superlattices*

In Fig. 9 we show the Raman spectrum of the [111] $CdTe/Cd_{0.75}Mn_{0.25}Te$ superlattice, SL-8, recorded at $T = 80$ K. The spectrum consists of only one Raman line in the frequency region of the MnTe-like phonon (peak A) and one in the region of the CdTe-like phonon (peak B), with Raman shifts not uniquely identified with the LO or TO phonons of either the well or the barrier layer; in contrast to the [001] superlattices, this is the case for all λ_L's. Peaks A and B appear in $z'(x'x')\bar{z}'$ (parallel polarization) as well as in $z'(y'x')\bar{z}'$ (crossed polarization), with a larger intensity in the parallel polarization. Here x', y', and z' are along $[01\bar{1}]$, $[2\,\bar{1}\,\bar{1}]$, and [111], respectively. A particularly noteworthy feature of these lines is their marked frequency dependence on λ_L; this is shown in Fig. 10 for SL-8 and SL-9.

For [111] $Cd_{1-x}Mn_xTe/Cd_{1-y}Mn_yTe$ superlattices, the point group symmetry is reduced to C_{3v} from the higher symmetry T_d of the bulk crystal. LO phonons with A_1 symmetry can be observed in $z'(x'x')\bar{z}'$ whereas TO phonons with E symmetry are allowed in both $z'(x'x')\bar{z}'$ and $z'(x'y')\bar{z}'$. The zone folding of propagating LO phonon referred to the new Brillouin zone can, in principle, show a small variation in its frequency as the energy of the incident laser radiation is changed. However, such a variation is expected to be insignificant in view of the highly dispersive character of those LO phonons likely to be observed. Furthermore, the behavior of Raman peak A is even more difficult to understand in this manner because its frequency increases with the incident photon energy, a behavior opposite to that expected for the folded LO phonons. Thus, there is a clear difference between Raman scattering from LO phonons in [111] and [001] superlattices.

In the light of the above observations, it is useful to review other experimental observations distinguishing these two types of superlattices. In Fig. 11, we show the

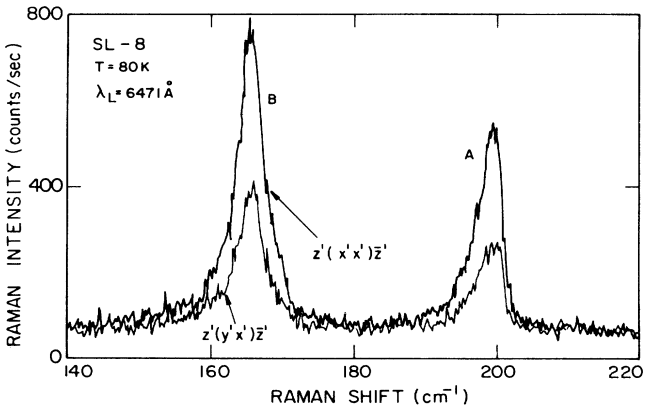

FIG. 9. Raman spectra in the frequency region of optical phonons in the $CdTe/Cd_{0.76}Mn_{0.24}Te$ superlattice SL-8, recorded at $T = 80$ K, for different polarizations. A and B are the Raman lines in the MnTe-like and CdTe-like phonon regions, respectively.

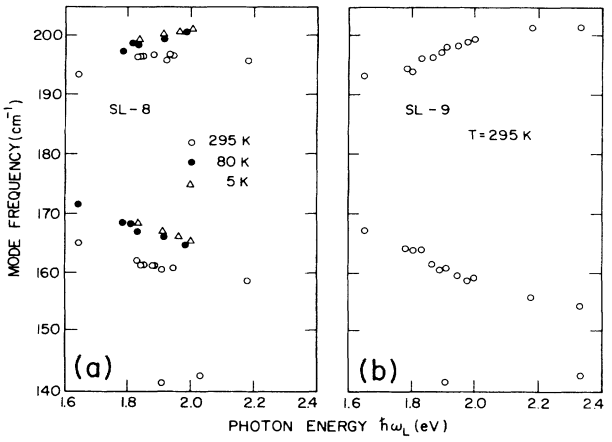

FIG. 10. The frequency variation of Raman lines in [111] $CdTe/Cd_{1-y}Mn_yTe$ as a function of the incident photon energy $\hbar\omega_L$. (a) SL-8 at 5, 80, and 295 K. (b) SL-9 at 295 K.

photoluminescence peak at $T=5$ K and magnetic fields of 0 and 60 kG in [111] $Cd_{0.89}Mn_{0.11}Te/Cd_{0.50}Mn_{0.50}Te$ superlattice, SL-4. The position of the luminescence peak shifts with magnetic field towards lower energy with an effective g factor of ~ 100. This demonstrates that the s-d and p-d exchange enhanced g factor characterizes the DMS superlattices[4] just as they do the bulk DMS's.[37] This enhancement is both magnetic field and temperature dependent. Furthermore, there is a marked difference between the magnetic field dependence of the photoluminescence spectrum in [111] and [001] superlattices, as was first reported in Ref. 38. The luminescence spectrum of [111] superlattices exhibits one broad peak arising from the excitons localized at the heterointerfaces, while for [001] superlattices, a sharp peak due to intrinsic excitons as well as a weaker one arising from the localized excitons were observed. It appears that a significantly larger number of excitons are localized at the heterointerfaces in the [111] than in the [001] superlattices. A result of this localization is the observed shift in the exciton luminescence peak position as the magnetic field is changed from being perpendicular to parallel with respect to the superlattice axis. In Fig. 12, we show a similar result for SL-4. From the large spectral red shift of the luminescence peak seen in other [111] superlattices, the authors of Ref. 38 argued that the excitons are localized at the interfaces, conceivably due to the compositional fluctuation at the interface. In addition, a TEM evaluation of the superlattice structure indicates that [111] samples have a surface dislocation density approximately an order of magnitude higher than in the [001] samples.[7] It also appears that the [001] interfaces are more abrupt than the [111] interfaces. We suggest that the quality of the interface results in the absence of confined or folded optical phonons in [111] superlattices and the Raman lines A and B should be ascribed to vibrations associated with the interface. The imperfection of the interfaces suggests the possibility of the excitation of IF modes even in the backscattering experiment in [111] superlattices. Furthermore, the observation of the exciton localization at the interfaces suggests that the IF mode may be strongly enhanced, thereby dominating the Raman spectra in these [111] superlattices.

IF modes have recently been observed in the Raman spectra of $GaAs/Ga_{1-x}Al_xAs$ superlattices and discussed in terms of an electrostatic model.[29] The dispersion relation for IF modes in a superlattice is given by[39]

$$\cos(q_z D)=\left[\frac{\eta^2+1}{2\eta}\right]\sinh(q_\perp d_1)\sinh(q_\perp d_2)+\cosh(q_\perp d_1)\cosh(q_\perp d_2)\ , \tag{2}$$

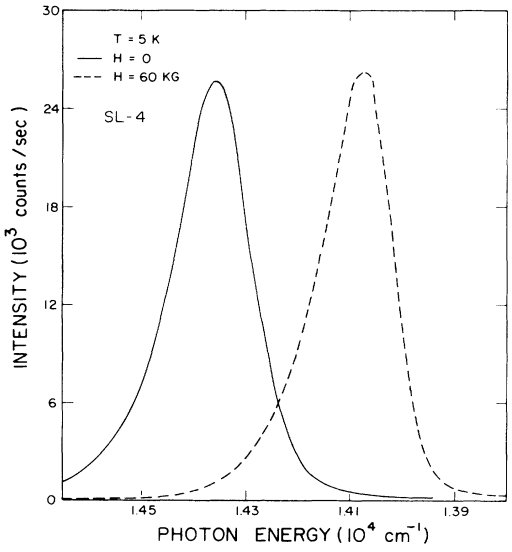

FIG. 11. Magnetic-field-induced shift in the position of the luminescence peak in $Cd_{0.89}Mn_{0.11}Te/Cd_{0.50}Mn_{0.50}Te$ superlattice, $\lambda_L=5682$ Å.

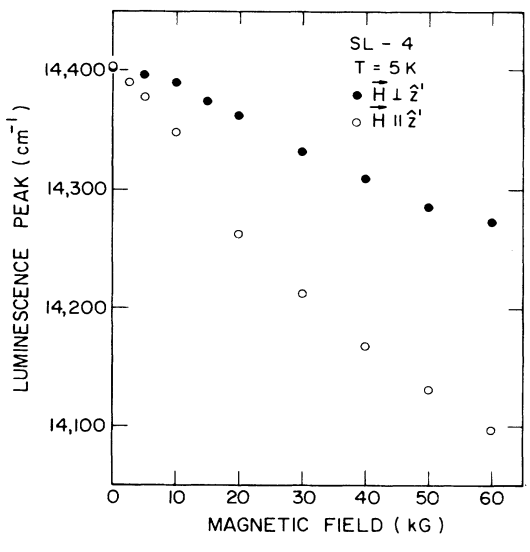

FIG. 12. Magnetic-field-induced shift in the position of the luminescence peak in $Cd_{0.89}Mn_{0.11}Te/Cd_{0.50}Mn_{0.50}Te$ with the magnetic field directions parallel or perpendicular to the superlattice axis.

where q_z and $q_\perp$ are the IF phonon wave vectors parallel and perpendicular to the superlattice axis, respectively. Even in the backscattering configuration, $q_\perp$ may not vanish if the interfaces are not perfect, thus allowing the IF phonons to be excited. In Eq. (2), $\eta=\epsilon_1(\omega)/\epsilon_2(\omega)$ is the ratio of the frequency-dependent dielectric constant of the well and barrier layers. For pure CdTe, the frequency-dependent dielectric constant is

$$\epsilon(\omega)=\epsilon(\infty)\frac{\omega^2-\omega_{\mathrm{LO}}^2}{\omega^2-\omega_{\mathrm{TO}}^2}\ , \tag{3}$$

whereas the $Cd_{1-x}Mn_xTe$ alloy, which exhibits a two-mode behavior, the dielectric constant is given by

$$\epsilon(\omega)=\epsilon(\infty)\frac{(\omega^2-\omega_{\mathrm{LO1}}^2)(\omega^2-\omega_{\mathrm{LO2}}^2)}{(\omega^2-\omega_{\mathrm{TO1}}^2)(\omega^2-\omega_{\mathrm{TO2}}^2)}\ . \tag{4}$$

In the above equations, ω_{LO} and ω_{TO} are the LO and TO phonon frequencies for CdTe and ω_{LO1}, ω_{TO1}, ω_{LO2}, and ω_{TO2} are the LO and TO phonon frequencies of CdTe-like and MnTe-like modes for $Cd_{1-x}Mn_xTe$, respectively. Equation (2) shows that an excitation is allowed in the frequency range for which η is negative. Hence, a superlattice consisting of pure CdTe layers alternating with $Cd_{1-x}Mn_xTe$ layers, as in SL-8 and SL-9, has IF modes in three frequency ranges: viz., ω_{TO1} to ω_{TO}; ω_{LO1} to ω_{LO}; and ω_{TO2} to ω_{LO2}. A superlattice characterized by $Cd_{1-x}Mn_xTe/Cd_{1-y}Mn_yTe$, $x\neq0$, $y\neq0$, has four regions of IF modes since both components now exhibit a two-mode behavior. In order to identify physically meaningful characteristics of the IF mode, we have calculated the frequency as a function of the wave vector q_z using Eq. (2). In Fig. 13, we show the frequencies of the Raman lines A, B, and C as well as the dispersion curves of IF modes calculated for a specific value of the wave vector parallel to the interface plane, viz., $q_\perp=0.2/d_1$, for SL-9; as the $q_\perp$ varies the slope of the dispersion curves will change slightly. Here (+) and (−) refer to the modes associated with the symmetric or antisymmetric potential with respect to the center of the layers, respectively. Based on the symmetric nature of the electronic wave function with respect to the center of the layers, it has been argued[29] that in Raman scattering the symmetric mode couples more strongly to the exciton via the intraband Fröhlich electron-phonon interaction. As we see in Fig. 13, although the observed range of the frequency variation exceeds that expected from the calculations, the functional behavior of the frequency variation with respect to the incident photon energy is consistent with theory. Similar phenomena have been observed in GaAs/$Ga_{1-x}Al_xAs$ superlattices,[30] in which only an IF mode was observed in the frequency region of an AlAs-like phonon. It therefore appears reasonable to conclude that the Raman lines observed in SL-8 and SL-9 are indeed IF modes.

When the incident laser excitation energy is increased to a value far from resonance, a prominent peak around 127 cm^{-1}, labeled D, as well as a peak labeled C in the vicinity of the TO phonon, were observed in addition to A and B as shown in Fig. 14. The longitudinal acoustic pho-

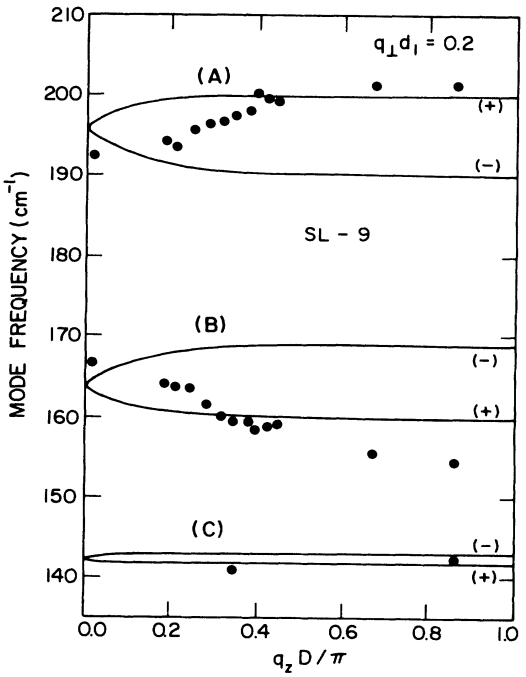

FIG. 13. Comparison of the frequency variation of observed Raman lines with the dispersion curves for interface vibrational modes in SL-9. (+) and (−) represent the modes associated with the potentials symmetric or antisymmetric with respect to the center of the layers; q_z and $q_\perp$ are the wave vectors of the interface phonons along and normal to the superlattice axis, respectively. Note that the new Brillouin zone is extremely small because of the large periodicity, $D=1300$ Å, for this superlattice. With laser wavelengths $5145\leq\lambda_L\leq7525$ Å, the phonon wave vector $q_z\cong4\pi n/\lambda_L$ has values between $2\pi/D$ and $3\pi/D$, which are equivalent to those between 0 and π/D.

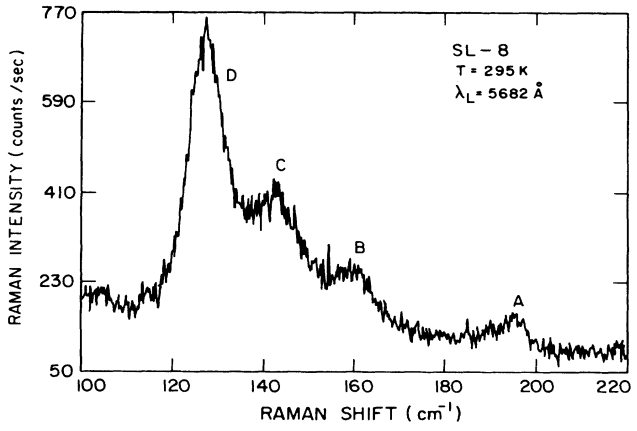

FIG. 14. Off-resonance Raman spectrum of SL-8 excited with $\lambda_L=5682$ Å. D is attributed to the disorder activated zone-boundary phonons, whereas A, B, and C are the Raman lines assigned to the interface modes as in Figs. 9 and 13.

nons in CdTe (Ref. 40) at the X point of its Brillouin zone, i.e., the LA(X) phonons, occur $\simeq 125$ cm^{-1}. The strong low-frequency feature D in the [111] superlattices could thus correspond to Raman scattering from disorder activated zone-boundary LA phonons selectively favored due to the large density of states. This could be construed as additional evidence of disorder in the [111] samples.

We now consider the results of Raman scattering in SL-4, a $Cd_{0.89}Mn_{0.11}Te/Cd_{0.50}Mn_{0.50}Te$ superlattice, which are different from those expected for either IF modes or bulk excitations. We have observed three Raman lines, one each in the frequency range corresponding to the MnTe-like phonons, the CdTe-like LO phonons, and the CdTe-like TO phonons. The frequencies of these peaks are shown as a function of incident photon energies in Fig. 15. Here, the frequencies of bulk zone-center optical-phonon modes for both the well and barrier components are shown by horizontal lines. The shaded ranges are the frequency regions where η is negative, allowing the excitation of an IF mode. As can be seen in Fig. 15, the Raman line in the frequency range of CdTe-like LO and TO phonons appears in the allowed frequency ranges for IF modes. On the other hand, the peak in the region of MnTe-like phonons can be identified neither with optical phonons nor with IF modes. Because of the relatively large difference in the Mn^{2+} concentrations of the well and barrier layers, the strain resulting from the lattice mismatch between the two layers is larger than in the other $CdTe/Cd_{1-x}Mn_xTe$ superlattices, SL-8 and SL-9. Such a strain can shift the frequencies of the optical phonons by a small amount, the sign of the frequency shift for each phonon being indicated by arrows in Fig. 15. However, the effect of the strain does not provide an explanation for the frequencies of the observed peaks since the frequency ranges of IF modes increase or decrease only by a small amount as shown in the figure. In order to have a definitive interpretation of the peaks observed in SL-4, further work with [111] superlattices having a wide range of d_1, d_2, x, and y is needed.

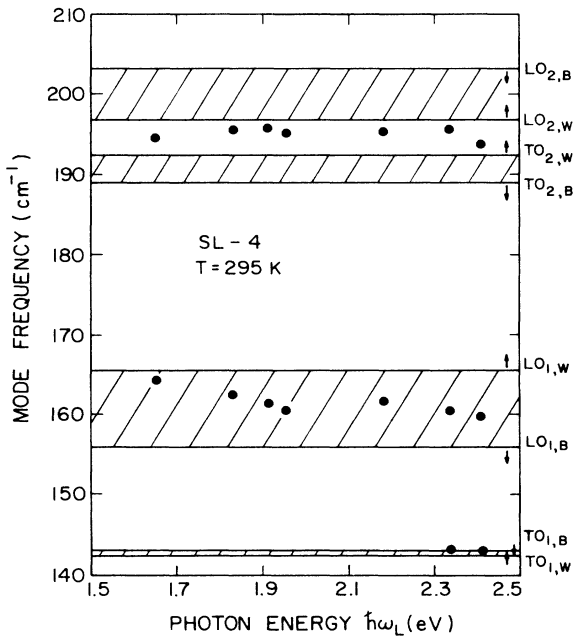

FIG. 15. Variation of the frequencies of the interface Raman lines in SL-4 as a function of the incident photon energy. The frequencies of bulk optical phonons corresponding to the well or barrier compositions are identified by horizontal lines. Subscripts 1 and 2 refer to CdTe-like and MnTe-like phonons, respectively, and B and W denote barrier and well components, respectively. The arrows show the direction in which the frequency shifts as a result of the strain due to lattice mismatch. The interface phonons are allowed in the shaded frequency ranges.

Finally, we discuss the resonant Raman effect of optical phonons in $Cd_{1-x}Mn_xTe/Cd_{1-y}Mn_yTe$ superlattices. We can obtain a resonance enhancement of optical phonons or of IF modes by matching the incident (in resonance) or the scattered (out resonance) photon energy with the electronic transitions in the superlattice. Exploiting the magnetic field dependence of the exciton photoluminescence peak with its large effective g factor as demonstrated in Fig. 11, we can achieve an out resonance either by magnetic field or by temperature tuning. This is illustrated in Figs. 16 and 17. In Fig. 16, we show the striking resonance effects observed for the Raman lines A and B in SL-4 with a magnetic field of 60 kG which shifts the onset of the photoluminescence peak to the region beyond 600 cm^{-1}. The clear observation of overtones and combinations of the two fundamental modes up to fourth order in these superlattices attests to the resonance enhancement. Similar resonant scattering is observed in SL-8 as shown in Fig. 17, where the onset of the photoluminescence peak lies beyond 900 cm^{-1} at zero magnetic field at $T = 80$ K. When the laser excitation energy is below the electronic transition energy none of these overtones is observed. Since the IF modes are associated with a macroscopic electric field, the striking out resonance seen in the parallel polarization suggests the coupling of these peaks with excitons localized at the interfaces, e.g.,

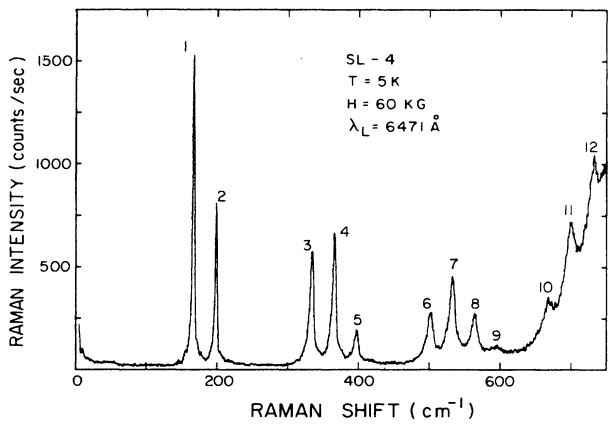

FIG. 16. Resonant Raman scattering from interface optical phonons, their overtones and combinations. The line labels denote the following assignments: (1) IF_1, (2) IF_2, (3) $2IF_1$, (4) IF_1+IF_2, (5) $2IF_2$, (6) $3IF_1$, (7) $2IF_1+IF_2$, (8) IF_1+2IF_2, (9) $3IF_2$, (10) $4IF_1$, (11) $3IF_1+IF_2$, (12) $2IF_1+IF_2$. IF_1 and IF_2 are the Raman lines B and A in [111] superlattices.

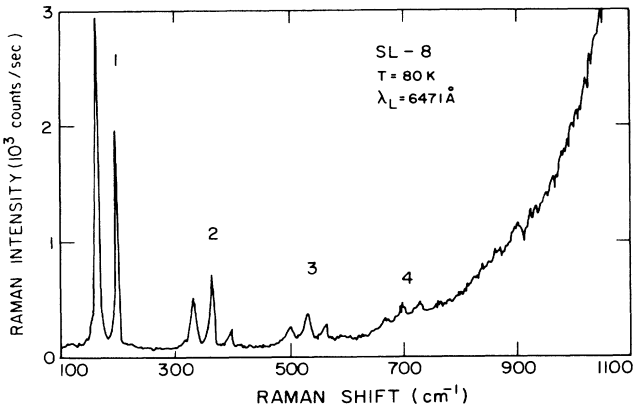

FIG. 17. Resonant Raman scattering from fundamental IF phonons, their overtones, and combinations in SL-8. Up to fourth-order overtones and combinations are clearly seen.

via the Fröhlich electron-phonon interaction.[41] The enhancement of the interface modes once more underscores the exciton localization in the interfaces in the [111] superlattices. Recently, resonant Raman scattering by combinations and overtones of IF phonons has also been observed in GaAs/AlAs superlattices.[42]

3. *ZnSe/$Zn_{1-x}Mn_xSe$ superlattices*

As we discussed in Sec. III B, the LO_1 phonon of $Zn_{1-x}Mn_xSe$ evolves continuously from the LO mode of ZnSe into that of MnSe with its frequency increasing with x. One thus expects the LO_1 phonon from $Zn_{1-x}Mn_xSe$ to be confined to the barrier layer while that from the ZnSe well propagates through both layers. We have examined five ZnSe/$Zn_{1-x}Mn_xSe$ superlattices with $0.23 \leq x \leq 0.51$, $24 \leq d_1 \leq 97$ Å, and $104 \leq d_2 \leq 180$ Å. The free-exciton transition in the zinc-blende $Zn_{1-x}Mn_xSe$ is in the range 2.7–3.1 eV at room temperature.[43] Thus the 4579-Å line of the Ar^+ laser is a convenient choice for exploiting the resonance enhancement associated with the electronic transitions in the ZnSe wells of these superlattices. In Fig. 18, the fundamental and the first overtone of the ZnSe LO phonon are clearly observed in the Raman spectrum of ZSL-3 for $\lambda_L = 4579$ Å; when the incident photon energy is close to the electronic transition of the well, the LO phonon of the ZnSe well and its overtone dominate the Raman spectrum. In order to simultaneously observe the LO phonons from the ZnSe well and from the $Zn_{1-x}Mn_xSe$ barrier layer, we chose $\lambda_L = 4880$ Å having an incident photon energy below the electronic transition energy. In Figs. 19(a) and 19(b) such off-resonance Raman spectra of LO phonons are presented for ZSL-3 and ZSL-12; both superlattices have ZnSe well and $Zn_{0.67}Mn_{0.33}Se$ barrier layers. In all the ZnSe/$Zn_{1-x}Mn_xSe$ superlattices or in the $Zn_{1-x}Mn_xSe$ thin layers, the LO_2 mode originating from the Mn^{2+} impurity modes is not observed; the TO modes are forbidden in the scattering geometry used. In Fig. 19(a), three LO phonons at ~250, ~252.5, and ~258 cm^{-1} appear in addition to the LO of the GaAs substrate at 292 cm^{-1}. The

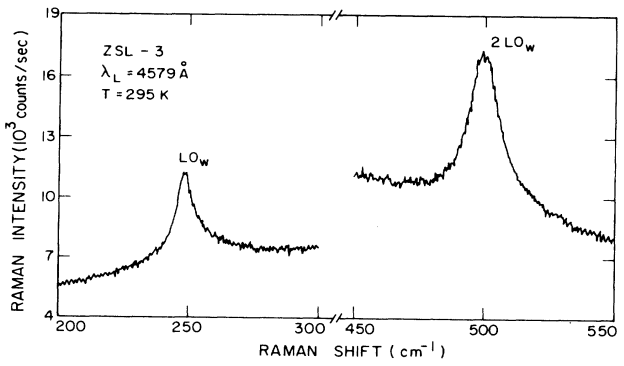

FIG. 18. Resonance Raman spectrum of the LO phonon of ZnSe well layers in ZSL-3. The fundamental and the overtone of LO_w are clearly seen.

highest-frequency phonon at ~258 cm^{-1} (LO_b) is from the $Zn_{1-x}Mn_xSe$ barrier. We note that the frequency of this phonon is shifted by ~3.5 cm^{-1} from the value of 254.5 cm^{-1} in the bulk crystal and in a thick $Zn_{0.67}Mn_{0.33}Se$ layer deposited on a GaAs substrate by MBE. Although this phonon is expected to be confined to the $Zn_{0.67}Mn_{0.33}Se$ layer, it is difficult to observe the other higher-order confined LO phonons, presumably due to the large layer thickness and the small difference in the frequencies between LO phonons of ZnSe and $Zn_{0.67}Mn_{0.33}Se$.[23] In addition, the frequency shift due to the confinement effect can be considered to be negligible in

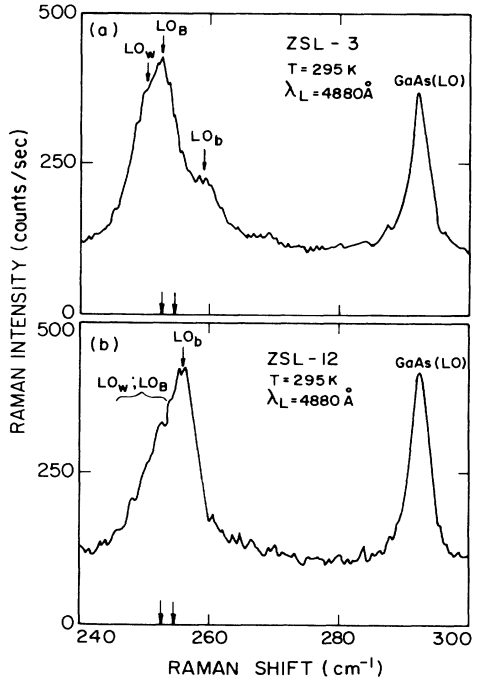

FIG. 19. Off-resonance Raman spectra of LO phonons in ZnSe/$Zn_{0.67}Mn_{0.33}Se$ superlattices. (a) ZSL-3 and (b) ZSL-12. Subscripts w, b, and B represent well, barrier, and buffer layers, respectively. The frequencies of LO phonons in bulk ZnSe and $Zn_{0.67}Mn_{0.33}Se$ are marked with arrows on the abscissas.

view of the larger barrier thickness. The position of phonons in the bulk crystals having the same compositions[23] as those of the well and barrier layers are marked by arrows on the abscissas in Fig. 19. The peaks labeled LO_w and LO_B were better resolved when a finer resolution was used and have frequencies of ~ 250 and ~ 252.5 cm^{-1}, respectively; we interpret them as the LO phonons of the ZnSe well layer and buffer layer, respectively. We note LO_B occurs at approximately the same frequency as that of the bulk crystal, while LO_w appears to be shifted by ~ 2.5 cm^{-1} to a lower frequency. Thus the positions of LO_b and LO_w indicate that there is a finite strain in the superlattice. The spectra for ZSL-2 and ZSL-4 are similar to that for ZSL-3. It seems reasonable to ascribe the frequency shifts of LO phonons in these superlattices, with respect to their positions in the bulk, to strain originating from the large lattice mismatch between the constituent layers.

Firstly, we note that the lattice mismatch between the wells and the barriers in superlattices is accommodated by a homogeneous strain. The magnitude of this strain depends on the effective lattice constant of the superlattice determined by the shear moduli and the lattice constants of both layers.[44] If we take into account the presence of the buffer layer but neglect the difference in the elastic constants of the barrier and the well, the effective lattice constant in the planes perpendicular to the superlattice axis is given by[45]

$$a_{\perp}^{\text{eff}}=\frac{n(a_w d_w+a_b d_b)+a_B d_B}{n(d_w+d_b)+d_B} , \tag{5}$$

where n is the number of periods, d's and a's with the subscripts w, b, and B are the layer thicknesses and the bulk lattice constants of the well, barrier, and buffer layer, respectively. In $ZnSe/Zn_{1-x}Mn_xSe$ superlattices, the ZnSe ($Zn_{1-x}Mn_xSe$) layer has an effective hydrostatic tensile (compressive) strain in the layer plane and an uniaxial compressive (tensile) strain along the growth axis. The strain in the layer plane is

$$\varepsilon_{xx}^i=\varepsilon_{yy}^i=\varepsilon_{\perp}^i=\frac{a_{\perp}^{\text{eff}}-a_i}{a_i} \tag{6}$$

and the strain in a direction parallel to the superlattice axis is

$$\varepsilon_{zz}^i=2\frac{s_{12}^i}{s_{11}^i+s_{12}^i}\varepsilon_{\perp}^i=-2\frac{c_{12}^i}{c_{11}^i}\varepsilon_{\perp}^i , \tag{7}$$

where i represents the well or barrier layers, and s_{ij} and c_{ij} are the elastic compliance and stiffness constants, respectively. Using these equations we can estimate the amount of the strain present in our superlattices. For example, in the superlattice used in Fig. 19(a), ZSL-3, containing a 2200-Å ZnSe buffer layer followed by a 175-Å $Zn_{1-x}Mn_xSe$ barrier and a 97-Å ZnSe well, the amount of the strain in each layer is estimated to be 0.0089 and -0.0066 for the well and barrier layer, respectively. Exciton ground-state splittings, which can be attributed to such strain, in $ZnSe/Zn_{1-x}Mn_xSe$ superlattices have been indeed observed.[45,46]

Secondly, the effect on the optical-phonon frequencies arising from the two-dimensional (2D) stretch or compression due to the lattice mismatch can be understood qualitatively in terms of such uniaxial strains.[47] Under a uniaxial strain, the frequency of optical phonons in the zinc-blende crystal shows a splitting and a shift.[48,49] The change in the frequency of the optical phonons in the presence of strain can be considered as the sum of a hydrostatic shift ($\Delta\Omega_H$) and a splitting ($\Delta\Omega$) due to the shear component of the stress. In the [001] $ZnSe/Zn_{1-x}Mn_xSe$ superlattices, the LO phonon observed in the backscattering configuration has a wave vector along the direction of the uniaxial strain, [001], and thus has an eigenvalue of the singlet component,[49] $\Omega_{\text{LO}}=\omega_{\text{LO}}+\delta\omega_{\text{LO}}$ with

$$\delta\omega_{\text{LO}}=\frac{p}{2\omega_{\text{LO}}}\varepsilon_{zz}+\frac{q}{2\omega_{\text{LO}}}2\varepsilon_{\perp}\equiv\Delta\Omega_H+\tfrac{2}{3}\Delta\Omega , \tag{8}$$

where Ω_{LO} and ω_{LO} are the frequencies of the LO phonon with and without the strain, respectively. In Eq. (8) the hydrostatic shift $\Delta\Omega_H$ and the splitting term $\Delta\Omega$ are

$$\Delta\Omega_H=-2\gamma\omega_{\text{LO}}\frac{c_{11}-c_{12}}{c_{11}}\varepsilon_{\perp} , \tag{9}$$

$$\Delta\Omega=-\frac{p-q}{2\omega_{\text{LO}}}\frac{c_{11}+2c_{12}}{c_{11}}\varepsilon_{\perp} , \tag{10}$$

where γ is the mode Grüneisen parameter, and p and q are the deformation constants. The mode Grüneisen parameters for LO and TO phonons in $Zn_{1-x}Mn_xSe$ for various x have been obtained from Raman scattering[23] under hydrostatic stress accessible with a diamond anvil cell; for LO phonons it is 0.79 and 1.02 for ZnSe and $Zn_{0.67}Mn_{0.33}Se$, respectively. Using the values of γ and $p-q$ for bulk ZnSe,[48] we estimate frequency shift of LO_w in ZSL-3 with respect to the frequency of the LO mode in bulk ZnSe to be ~ -2.8 cm^{-1}, showing a good agreement with that observed. The deformation constants for $Zn_{1-x}Mn_xSe$ have not yet been determined. However, we can estimate $(p-q)/2\omega_{\text{LO}}^2$ from the observed frequency shift of LO_b using Eqs. (8)–(10); it is ~ 0.98, significantly larger than that for ZnSe.[50] In this context, it is clearly of interest to perform Raman scattering measurements on $Zn_{1-x}Mn_xSe$ under uniaxial stress.

In Fig. 19(b), we show the Raman spectrum of another $ZnSe/Zn_{0.67}Mn_{0.33}Se$ superlattice (ZSL-12). In contrast to ZSL-3, this superlattice has a pure ZnSe buffer layer followed by a $Zn_{0.67}Mn_{0.33}Se$ buffer layer. Therefore we expect four peaks in the LO phonon region; LO_w, LO_b, and two LO_B's: one corresponding to ZnSe buffer and the other from the $Zn_{0.67}Mn_{0.33}Se$ buffer layer. They are not well resolved as we see in Fig. 19(b). However, we note that the highest-frequency phonon LO_b is approximately at 256 cm^{-1} showing a smaller shift than that for ZSL-3, as can be seen from a comparison of Figs. 19(a) and 19(b). The strains in the superlattice estimated using Eqs. (5) and (6) are 0.0127 in the ZnSe layer and -0.0028 in the $Zn_{0.67}Mn_{0.33}Se$ layer for ZSL-12, approximately half of the strain in the $Zn_{0.67}Mn_{0.33}Se$ layer as compared with $Zn_{0.67}Mn_{0.33}Se$ layer in ZSL-3. This difference in strain is

consistent with the difference in the observed frequency shifts of LO_b with respect to the LO_1 of bulk $Zn_{0.67}Mn_{0.33}Se$ as manifested in the two superlattices; the estimated frequency shift of LO_b in ZSL-12 using $(p-q)/2\omega_{LO}^2=0.98$ for $Zn_{0.67}Mn_{0.33}Se$ as obtained above is ~ 1.5 cm^{-1}, showing an excellent agreement with the observed frequency shift as can be seen in Fig. 19(b).

C. Magnetic excitations

In this section we discuss magnetic excitations in DMS superlattices. Bulk DMS alloys exhibit a magnetic phase transition as the temperature is lowered and the Mn^{2+} concentration increases. Using specific-heat and magnetic susceptibility measurements, it has been found[51] that $Cd_{1-x}Mn_xTe$ crystals are paramagnetic at $T \geq 5$ K for $x \lesssim 0.17$, but as the temperature is lowered the crystal shows a transition from paramagnetic to a magnetically ordered phase depending on x.

In the paramagnetic phase, Raman scattering associated with spin-flip transitions between adjacent sublevels of Zeeman multiplet of the ground state of Mn^{2+} has been observed in an external magnetic field in bulk $Cd_{1-x}Mn_xTe$ crystals.[52] Such Raman lines are also observed in DMS superlattices, as can be seen in Fig. 20. With an applied magnetic field of 60 kG, an intense Raman paramagnetic resonance signal (PM) as well as multiple spin-flip Raman peaks up to fifth order are observed when the incident photon energy resonates with the excitonic transitions. Multiple spin-flip Raman scattering has also been observed in the bulk and is accounted for in terms of excitations within antiferromagnetically coupled Mn^{2+} ion pairs.[27] In addition, as in the bulk, coupling between the Mn^{2+} spin-flip transition and vibrational excitations is also observed in superlattices. In Fig. 21, in the Raman spectrum of the [111] superlattice, SL-4, Raman lines A, B, and their combinations with PM are seen with a laser excitation energy close to the electronic transitions of the well layers. The peaks labeled as "A +PM" and "B +PM" are a result

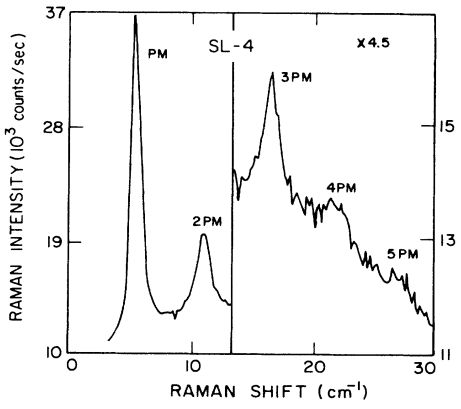

FIG. 20. Raman scattering associated with the paramagnetic spin-flip transitions (ω_{PM}) in the [111] $Cd_{0.89}Mn_{0.11}Te/Cd_{0.50}Mn_{0.50}Te$ superlattice SL-4. Exciting wavelength $\lambda_L=6764$ Å, $P_L=10$ mW, the applied magnetic field $H=60$ kG, and temperature $T=5$ K.

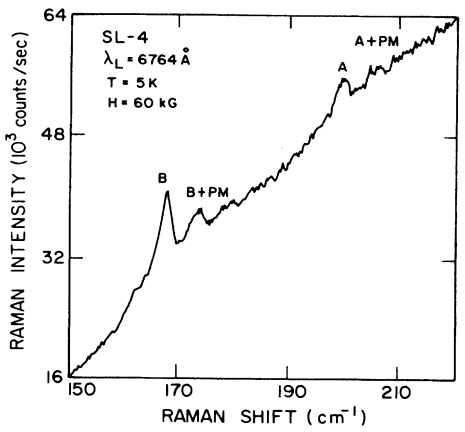

FIG. 21. Raman spectrum of SL-4 with $H=60$ kG, showing Raman lines A, B, and their combinations with PM. The sloping background is due to photoluminescence.

of the creation of interface phonons through the Fröhlich interaction[21] during which there is a simultaneous excitation of the Mn^{2+} ion to the next sublevel of the Zeeman multiplet. Similar Raman lines are observed in SL-8.

For bulk $Cd_{1-x}Mn_xTe$ crystals in the magnetically ordered phase, a zero-field magnetic excitation (magnon) associated with the Mn^{2+} ions has been observed.[21] As the temperature is lowered the Mn^{2+} spin flip of the paramagnetic phase evolves into the high-frequency component of the magnon doublet of the spin-glass phase. As in the case of the optical phonons, we can expect to observe confined or propagating magnons depending upon the Mn^{2+} concentrations of the superlattice layers. In addition, we also expect a magnetic excitation propagating along the interface with an amplitude decaying exponentially along the superlattice axis, similar to the IF phonons. The dispersion relation for such magnetic excitations is derived in the Appendix.

The superlattices we have examined have barrier layers of DMS alloys which exhibit magnetic ordering for $T \leq 5$ K, in the bulk crystal. Thus one can expect to observe magnons confined in the barrier layers as well as those propagating along the interfaces at low temperature. However, we have not yet observed any feature which we can associate with such modes in either backscattering or right-angle scattering. It is possible that even at 1.8 K the two-dimensional thin layers of the superlattice may lack spin-glass ordering, even though such ordering occurs for the same composition of the bulk alloy. If so, this would signify that the dimensional constraints created in a superlattice can exert a decisive influence on magnetic phase transitions. Recently, Gunshor *et al.*[53] have come to similar conclusions on the basis of their studies on the Zeeman effect of the photoluminescence of the ZnSe/MnSe superlattice. In this context, it is of interest to perform specific-heat and magnetic susceptibility measurements on DMS superlattices.

Finally, we note that Raman scattering from antiferromagnetically coupled Mn^{2+} ion pairs has been observed in the bulk $Cd_{1-x}Mn_xSe$ and $Cd_{1-x}Mn_xS$,[54] both of

which have wurtzite structure with C_{6v} point group symmetry. Antiferromagnetically coupled Mn^{2+} pairs possess a series of energy levels for the total spin $S=0$, 1, 2, 3, 4, and 5 states; the separation of the energy levels is determined by the nearest-neighbor exchange interaction $|J_{NN}|$. Raman lines associated with transitions between the spin multiplets have a temperature dependence characteristic of the population of the multiplets. We have observed a distinct Raman line at 9.5 ± 0.3 cm^{-1} in the [111] $Cd_{0.89}Mn_{0.11}Te/Cd_{0.50}Mn_{0.50}Te$ superlattice, SL-4, when the incident photon energy resonates with the electronic transitions of the well, as shown in Fig. 22. We ascribe this to the Raman line associated with the transition from the $S=0$ to the $S=1$ state of the Mn^{2+} pairs in $Cd_{0.89}Mn_{0.11}Te$ layers. This peak exhibits the same characteristics as those discussed in Ref. 54; the peak lacks any polarization characteristics, does not show any magnetic field dependence up to 60 kG, and its intensity decreases as the temperature increases. Its transition energy yields the nearest-neighbor exchange constant, $|J_{NN}|=6.8\pm0.2$ K, which agrees with previously determined values that range from 6.3 to 7.7 K.[55] It is particularly interesting to note that bulk $Cd_{1-x}Mn_xTe$, as well as the other DMS's of zinc-blende structure with point group symmetry T_d, do not show this Raman peak.[54] The appearance of the Mn^{2+} pair Raman peak in SL-4 could be due to the new crystal symmetry of the $Cd_{1-x}Mn_xTe$ layers; [111] superlattices have a crystal symmetry of point group C_{3v} and, in addition, have an uniaxial strain along the superlattice axis.

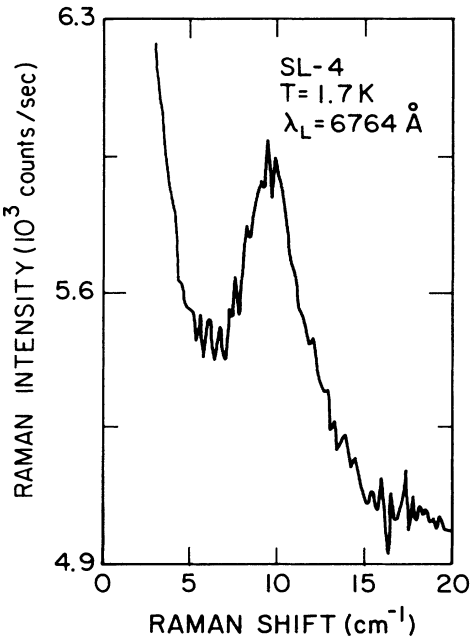

FIG. 22. Raman scattering associated with the spin-flip transitions from antiferromagnetically coupled Mn^{2+} ion pairs in $Cd_{0.89}Mn_{0.11}Te/Cd_{0.50}Mn_{0.50}Te$, SL-4; $T=1.7$ K, $P_L=10$ mW.

IV. CONCLUDING REMARKS

Our Raman scattering studies of DMS superlattices have led to the observation of a number of collective excitations characteristic of superlattices. However, further investigations are needed—and are indeed planned—to address specific aspects of these excitations and to discover those predicted but not yet experimentally observed. Specially designed heterostructures with parameters optimum for such observations will be fabricated in this context. We list below some of the problems of physical interest which are worthy of further studies.

(1) The possibility of growing tetrahedrally coordinated end members (e.g., MnTe and MnSe) of the DMS's offers the exciting possibilities of studying these hitherto hypothetical crystals; it will be of interest to compare the behavior of lattice dynamics and magnetic excitations directly in these structures with that extrapolated from the study of bulk crystals as a function of x.

(2) In order to take full advantage of the resonant Raman effect in $ZnSe/Zn_{1-x}Mn_xSe$ superlattices, further studies are needed using higher-energy laser radiation.

(3) The observation of folded transverse acoustic phonons will complement the studies of folded LA phonons; a high-resolution, high-contrast Fabry-Perot interferometer will be employed in such studies.

(4) The theory of magnetic excitations in DMS superlattices predicts excitations analogous to the IF vibrations of optical phonons, which can be studied with suitably designed superlattices in which the Mn^{2+} concentration is large in both layers.

ACKNOWLEDGMENTS

We wish to thank Professor N. Otsuka for the transmission-electron-microscopy characterization of the superlattices and Dr. A. K. Sood and Dr. A. K. Arora for stimulating discussions. This work is supported in part by the National Science Foundation Grant No. DMR-84-03325 (E.-K.S., D.U.B., A.K.R., and S.R.), U.S. Defense Advanced Projects Agency (DARPA/URI) Grant No. N00014-86-K-0760 awarded through the U.S. Office of Naval Research (ONR) and ONR Contract No. N-00014-82-K0563 (L.A.K. and R.L.G.). The program benefited from the Central Laser Facility operated under National Science Foundation Materials Research Laboratory, (NSF-MRL) Program Grant No. DMR-84-18453.

APPENDIX: INTERFACE MAGNETOSTATIC MODES

We consider the interface magnetization waves in a superlattice formed of two different materials, denoted by 1 and 2, as shown in Fig. 23. To fix our ideas we consider each component of the superlattice to contain a different concentration of magnetic atoms. We neglect the effect of retardation so that the magnetic fields obey the equations of magnetostatics, viz.,

$$\nabla\times\mathbf{H}=0\ ,$$

and

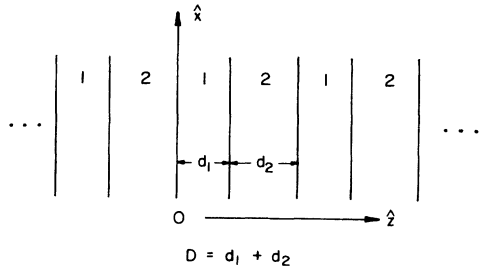

FIG. 23. Schematic diagram of a superlattice where 1 and 2 refer to well and barrier layers of thicknesses d_1 and d_2, respectively. $D=d_1+d_2$ is the superlattice period, $\hat{\mathbf{z}}$ the superlattice axis, and $\hat{\mathbf{x}}$ an axis on the layer plane.

$$\nabla\cdot\mathbf{B}=0 , \tag{A1}$$

where $\mathbf{H}=\mathbf{B}-4\pi\mathbf{M}$. Under such conditions a magnetic scalar potential ϕ_M can be defined such that the intensity of the magnetic field $\mathbf{H}$ is

$$\mathbf{H}=-\nabla\phi_M . \tag{A2}$$

Therefore

$$\nabla^2\phi_M=4\pi\nabla\cdot\mathbf{M} . \tag{A3}$$

Let there be an external magnetic field $H_0\hat{\mathbf{z}}$ parallel to the axis of the superlattice. We study magnetization modes in which the component of $\mathbf{M}$ parallel to $\hat{\mathbf{z}}$ is constant while that in the plane of the layers vibrates harmonically with angular frequency ω, i.e.,

$$\mathbf{M}=M_0\hat{\mathbf{z}}+\mathbf{M}_\perp e^{-i\omega t} . \tag{A4}$$

The equation of motion of the magnetization is the Bloch equation

$$\frac{d\mathbf{M}}{dt}=\gamma\mathbf{M}\times\mathbf{H} , \tag{A5}$$

where γ is the gyromagnetic ratio and the magnetic field is

$$\mathbf{H}=H_z\hat{\mathbf{z}}+\mathbf{H}_\perp e^{-i\omega t} . \tag{A6}$$

Taking $\mathbf{M}_\perp$ and $\mathbf{H}_\perp$ as small, we linearize the Bloch equation to obtain

$$-i\omega\mathbf{M}_\perp=\gamma M_0\hat{\mathbf{z}}\times\mathbf{H}_\perp+\gamma H_z\mathbf{M}_\perp\times\hat{\mathbf{z}} . \tag{A7}$$

Solving this equation for $\mathbf{M}_\perp$, we obtain

$$\mathbf{M}_\perp=-\frac{\gamma^2H_zM_0}{\omega^2-\gamma^2H_z^2}\mathbf{H}_\perp+\frac{i\omega\gamma M_0\hat{\mathbf{z}}\times\mathbf{H}_\perp}{\omega^2-\gamma^2H_z^2} . \tag{A8}$$

Substitution of Eq. (A8) into Eq. (A3) yields

$$\nabla^2\phi_M=4\pi\nabla\cdot\mathbf{M}_\perp=-\frac{4\pi\gamma^2H_zM_0}{\omega^2-\gamma^2H_z^2}\nabla\cdot\mathbf{H}_\perp . \tag{A9}$$

Thus

$$\mu(\omega)\left[\frac{\partial^2\phi_M}{\partial x^2}+\frac{\partial^2\phi_M}{\partial y^2}\right]+\frac{\partial^2\phi_M}{\partial z^2}=0 , \tag{A10}$$

where

$$\mu(\omega)=1-\frac{4\pi\gamma^2H_zM_0}{\omega^2-\gamma^2H_z^2} . \tag{A11}$$

We now investigate modes having

$$\phi_M=\psi(z)e^{i(q_xx+q_yy)-i\omega t} . \tag{A12}$$

The function $\psi(z)$ obeys the differential equation

$$\frac{d^2\psi}{dz^2}-\mu q_\perp^2\psi=0 \tag{A13}$$

with $q_\perp^2=q_x^2+q_y^2$. The solution of Eq. (A13) is

$$\psi(z)=Ae^{Qz}+Be^{-Qz} , \tag{A14}$$

where $Q=\sqrt{\mu}q_\perp$. For a superlattice in which $\mu(\omega)$ takes the values $\mu_1(\omega)$ and $\mu_2(\omega)$ in the layers of thicknesses d_1 and d_2, respectively,

$$\begin{aligned}\psi(z)&=A_1e^{Q_1z}+B_1e^{-Q_1z}, \quad 0\le z\le d_1\\ &=A_2e^{Q_2z}+B_2e^{-Q_2z}, \quad d_1\le z\le d_1+d_2=D .\end{aligned} \tag{A15}$$

The condition of continuity of the tangential component of $\mathbf{H}$ is equivalent to that of the continuity of ϕ_M and hence of ψ. The time-dependent normal component of $\mathbf{B}$ is simply $-\partial\phi_M/\partial z$. This quantity is, therefore, also continuous. In addition, as in the cases of optical and acoustical phonons,[56] $\psi(z)$ obeys the Bloch condition, $\psi(z+D)=e^{iq_zD}\psi(z)$ for wave vector q_z along $\hat{\mathbf{z}}$. These conditions yield

$$\begin{aligned}\cos(q_zD)=&\cosh(Q_1d_1)\cosh(Q_2d_2)\\ &+\frac{\mu_1(\omega)+\mu_2(\omega)}{2\sqrt{\mu_1(\omega)\mu_2(\omega)}}\sinh(Q_1d_1)\sinh(Q_2d_2) .\end{aligned} \tag{A16}$$

In the antiferromagnetic phase of a Mn-based DMS the relation between $\mathbf{M}_\perp$ and $\mathbf{H}_\perp$ obtained above is modified according to the following argument. We classify the magnetic moments of the Mn^{2+} ions into two classes pointing preferentially in opposite directions. The net magnetization of the two classes of atoms are denoted by $\mathbf{M}_1$ and $\mathbf{M}_2$. In equilibrium $\mathbf{M}_1+\mathbf{M}_2=\mathbf{0}$. However in a magnetic field of the form (A6), $\mathbf{M}_1$ and $\mathbf{M}_2$ vary according to

$$\frac{\partial\mathbf{M}_1}{\partial t}=\gamma\mathbf{M}_1\times(\mathbf{H}-\lambda\mathbf{M}_2+\mathbf{H}_A) , \tag{A17}$$

and

$$\frac{\partial\mathbf{M}_2}{\partial t}=\gamma\mathbf{M}_2\times(\mathbf{H}-\lambda\mathbf{M}_1-\mathbf{H}_A) . \tag{A18}$$

Here $\lambda\mathbf{M}_{1,2}$ is the exchange field due to atoms of class 1 (2) on atoms of class 2 (1) and $\mathbf{H}_A$ is an anisotropy field. To simplify the discussion we take $\mathbf{H}_A$ parallel to $H_z\hat{\mathbf{z}}$. We now write

$$\mathbf{M}_1=M_0\hat{\mathbf{z}}+\mathbf{M}_{1\perp}e^{-i\omega t} \tag{A19}$$

and

$$\mathbf{M}_2 = -M_0\hat{\mathbf{z}} + \mathbf{M}_{2\perp}e^{-i\omega t} . \tag{A20}$$

If we denote the exchange field by $H_E = \lambda M_0$, the Bloch equations yield (after keeping only linear terms in $\mathbf{M}_\perp$ and $\mathbf{H}_\perp$)

$$-i\omega\mathbf{M}_{1\perp} = \gamma M_0\hat{\mathbf{z}}\times\mathbf{H}_\perp - \gamma H_E\hat{\mathbf{z}}\times\mathbf{M}_{2\perp} - \gamma(H_0 + H_E + H_A)\hat{\mathbf{z}}\times\mathbf{M}_{1\perp} , \tag{A21}$$

and

$$-i\omega\mathbf{M}_{2\perp} = -\gamma M_0\hat{\mathbf{z}}\times\mathbf{H}_\perp + \gamma H_E\hat{\mathbf{z}}\times\mathbf{M}_{1\perp} - \gamma(H_0 - H_E - H_A)\hat{\mathbf{z}}\times\mathbf{M}_{2\perp} . \tag{A22}$$

We need to evaluate $\mathbf{M}_\perp = \mathbf{M}_{1\perp} + \mathbf{M}_{2\perp}$ in terms of $\mathbf{H}_\perp$. This is accomplished by adding and subtracting Eqs. (A21) and (A22), and eliminating $\mathbf{M}_{1\perp} - \mathbf{M}_{2\perp}$. We obtain

$$\mathbf{M}_\perp = \frac{bc}{a^2+b^2}\mathbf{H}_\perp + \frac{ac}{a^2+b^2}\hat{\mathbf{z}}\times\mathbf{H}_\perp , \tag{A23}$$

where

$$a = 2i\omega\gamma H_z ,$$

$$b = -\omega^2 - \gamma^2 H_z^2 + \gamma^2 H_A^2 + 2\gamma^2 H_A H_E ,$$

and

$$c = 2\gamma^2 M_0 H_A .$$

The vector potential ϕ_M satisfies again Eq. (A10) with μ replaced by

$$\mu = 1 + \frac{4\pi bc}{a^2+b^2} = 1 - \frac{8\pi\gamma^2 M_0 H_A(\omega^2 - \omega_+\omega_-)}{(\omega^2-\omega_+^2)(\omega^2-\omega_-^2)} , \tag{A24}$$

where

$$\omega_\pm = \pm\gamma H_z + |\gamma|(H_A^2 + 2H_A H_E)^{1/2} \tag{A25}$$

are the antiferromagnetic spin wave frequencies for long wavelengths. The condition of periodicity yields, as before, the result embodied in Eq. (A16). We now apply our analysis to the experiments discussed in this paper, where the layers have $x = 0.11$ and $y = 0.5$ for SL-4. In the bulk the well layer would be paramagnetic while the barrier layer would be in the magnetically ordered phase at the low temperature. Assuming right-angle scattering, say, with geometry $\bar{z}(xy)x$, and $Q_1 d_1, Q_2 d_2 \ll 1$ for $q_z D \simeq 2\pi n$ ($n = 0, \pm 1, \pm 2, \ldots$), we obtain

$$\mu_1 d_1 + \mu_2 d_2 = -D . \tag{A26}$$

Using Eqs. (A11) and (A24) one can find the frequency of the surface magnetic modes. In the absence of an external magnetic field, this frequency is given by

$$\omega^2 = \omega_M^2\left[1 + \frac{2\pi d_1}{\lambda D}\right] , \tag{A27}$$

where λ is the exchange parameter defined above. Since λ is of order 5×10^2 (Ref. 21) the correction in Eq. (A27) is negligible.

However, if both layers are in the paramagnetic phase with externally applied field H_z, Eqs. (A11) and (A26) yield

$$\omega^2 = \omega_{\mathrm{PM}}^2\left[1 + \frac{2\pi\chi}{D}(xd_1 + yd_2)\right] , \tag{A28}$$

where χ is the magnetic susceptibility for $x = 1$ and $\hbar\omega_{\mathrm{PM}} = |\gamma| H_z$. For high magnetic fields at low temperature χ is not linear. The correction term in Eq. (A28) is again negligible.

[1] L. A. Kolodziejski, T. C. Bonsett, R. L. Gunshor, S. Datta, R. B. Bylsma, W. M. Becker, and N. Otsuka, Appl. Phys. Lett. **45**, 440 (1984).

[2] L. A. Kolodziejski, R. L. Gunshor, N. Otsuka, X.-C. Zhang, S.-K. Chang, and A. V. Nurmikko, Appl. Phys. Lett. **47**, 882 (1985).

[3] R. N. Bicknell, R. Yanka, N. C. Giles-Taylor, D. K. Blanks, E. L. Buckland, and J. F. Schetzina, Appl. Phys. Lett. **45**, 92 (1984).

[4] S. Datta, J. K. Furdyna, and R. L. Gunshor, Superlatt. Microstruct. **1**, 327 (1985).

[5] D. R. Yoder-Short, U. Debska, and J. K. Furdyna, J. Appl. Phys. **58**, 4056 (1985).

[6] L. A. Kolodziejski, R. L. Gunshor, N. Otsuka, B. P. Gu, Y. Hefetz, and A. V. Nurmikko, Appl. Phys. Lett. **48**, 1482 (1986).

[7] R. L. Gunshor, L. A. Kolodziejski, N. Otsuka, S. K. Chang, and A. V. Nurmikko, J. Vac. Sci. Technol. A **4**, 2117 (1986).

[8] N. Otsuka, L. A. Kolodziejski, R. L. Gunshor, S. Datta, R. N. Bicknell, and J. F. Schetzina, Appl. Phys. Lett. **46**, 860 (1985).

[9] C. Colvard, R. Merlin, M. V. Klein, and A. C. Gossard, Phys. Rev. Lett. **45**, 298 (1980).

[10] J. Sapriel, J. C. Michel, J. C. Toledano, R. Vacher, J. Kervarec, and A. Regreny, Phys. Rev. B **28**, 2007 (1983).

[11] B. Jusserand, F. Alexandre, J. Dubard, and D. Paquet, Phys. Rev. B **33**, 2897 (1986).

[12] H. Brugger, G. Abstreiter, H. Jorke, H. J. Herzog, and E. Kasper, Phys. Rev. B **33**, 5928 (1986).

[13] P. Santos, M. Hundhausen, and L. Ley, Phys. Rev. B **33**, 1516 (1986).

[14] A preliminary report of our work appears in S. Venugopalan, L. A. Kolodziejski, R. L. Gunshor, and A. K. Ramdas, Appl. Phys. Lett. **45**, 974 (1984).

[15] S. M. Rytov, Akust. Zh. **2**, 71 (1956) [Sov. Phys.—Acoust. **2**, 68 (1956)].

[16] Elastic moduli of a single crystal of $Cd_{1-x}Mn_xTe$ with $x = 0.5$ were determined by Brillouin scattering experiment: A Petrou, S. Venugopalan, and A. K. Ramdas (unpublished).

[17] P. Maheswaranathan, R. J. Sladek, and U. Debska, Phys. Rev. B **31**, 5212 (1985).

[18] Elastic constants and densities for $Zn_{1-x}Mn_xSe$ bulk crystals were estimated from the values measured by R. Mayanovic

and R. J. Sladek. We have expressed the elastic constants for cubic symmetry in terms of those for wurtzite symmetry; the values for various x were obtained by interpolation.

[19]See, for example, W. B. Daniels, in *Lattice Dynamics*, edited by R. F. Wallis (Pergamon, Oxford, 1965), p. 273. For the pressure derivatives of the elastic stiffness moduli, see Ref. 17.

[20]C. Colvard, T. A. Gant, M. V. Klein, R. Merlin, R. Fischer, H. Morkoc, and A. C. Gossard, Phys. Rev. B **31**, 2080 (1985).

[21]S. Venugopalan, A. Petrou, R. R. Galazka, A. K. Ramdas, and S. Rodriguez, Phys. Rev. B **25**, 2681 (1982).

[22]D. L. Peterson, A. Petrou, W. Giriat, A. K. Ramdas, and S. Rodriguez, Phys. Rev. B **33**, 1160 (1986).

[23]Akhilesh K. Arora, E.-K. Suh, U. Debska, and A. K. Ramdas (unpublished).

[24]Recently, it has been pointed out that in GaAs/AlAs superlattices the atomic displacements do not vanish at the boundary of the GaAs layer but vanish at the first Al atoms in the neighboring AlAs layers. See, for example, A. K. Sood, J. Menendez, M. Cardona, and K. Ploog, Phys. Rev. Lett. **56**, 1753 (1986); B. Jusserand and D. Paquet, *ibid.* **56**, 1752 (1986).

[25]B. Jusserand, D. Paquet, and A. Regreny, Phys. Rev. B **30**, 6245 (1984).

[26]A. S. Barker, Jr. and R. Loudon, Rev. Mod. Phys. **44**, 18 (1972); J. E. Zucker, A. Pinczuk, D. S. Chemla, A. Gossard, and W. Wiegmann, Phys. Rev. Lett. **53**, 1280 (1984).

[27]D. L. Peterson, D. U. Bartholomew, A. K. Ramdas, and S. Rodriguez, Phys. Rev. B **31**, 7932 (1985).

[28]R. Fuchs and K. L. Kliewer, Phys. Rev. **140**, A2076 (1965); G. Kanellis, J. F. Morhange, and M. Balkanski, Phys. Rev. B **28**, 3406 (1983).

[29]A. K. Sood, J. Menendez, M. Cardona, and K. Ploog, Phys. Rev. Lett. **54**, 2115 (1985).

[30]A. K. Arora, A. K. Ramdas, M. R. Melloch, and N. Otsuka, Phys. Rev. B **36**, 1021 (1987).

[31]Ph. Lambin, J. P. Vigneron, A. A. Lucas, P. A. Thiry, M. Liehr, J. J. Pireaux, R. Caudano, and T. J. Kuech, Phys. Rev. Lett. **56**, 1842 (1986).

[32]N. Bottka, J. Stankiewicz, and W. Giriat, J. Appl. Phys. **52**, 4189 (1981).

[33]L. A. Kolodziejski, R. L. Gunshor, R. Venkatasubramanian, T. C. Bonsett, R. Frohne, S. Datta, N. Otsuka, R. B. Bylsma, W. M. Becker, and A. V. Nurmikko, J. Vac. Sci. Technol. B **4**, 583 (1986).

[34]A. S. Barker, Jr., J. L. Merz, and A. C. Gossard, Phys. Rev. B **17**, 3181 (1978).

[35]A. K. Sood, J. Menendez, M. Cardona, and K. Ploog, Phys. Rev. Lett. **54**, 2111 (1985).

[36]Strictly speaking, the strain in this lattice-mismatched superlattice will also lower the frequency of this peak. However, the effect of strain is not large in this superlattice as we can see from the frequency in the CdTe-like phonon which is almost the same as that of bulk $Cd_{0.75}Mn_{0.25}Te$. Therefore we will not consider the effect of strain in $CdTe/Cd_{1-x}Mn_xTe$ superlattices.

[37]J. K. Furdyna, J. Vac. Sci. Technol. A **4**, 2002 (1986).

[38]X.-C. Zhang, S.-K. Chang, A. V. Nurmikko, L. A. Kolodziejski, R. L. Gunshor, and S. Datta, Phys. Rev. B **31**, 4056 (1986); X.-C. Zhang, S.-K. Chang, A. V. Nurmikko, D. Heiman, L. A. Kolodziejski, R. L. Gunshor, and S. Datta, Solid State Commun. **56**, 255 (1985); S.-K. Chang, A. V. Nurmikko, L. A. Kolodziejski, and R. L. Gunshor, Phys. Rev. B **33**, 2589 (1986).

[39]See, for example, E. P. Pokatilov and S. I. Beril, Phys. Status Solidi B **110**, K75 (1982); R. E. Camley and D. L. Mills, Phys. Rev. B **29**, 1695 (1984).

[40]J. M. Rowe, R. M. Nicklow, D. L. Price, and K. Zanio, Phys. Rev. **10**, 671 (1974).

[41]See, for example, M. Cardona, in *Light Scattering in Solids II*, Vol. 50 of *Topics in Applied Physics*, edited by M. Cardona and G. Güntherodt (Springer, Berlin, 1982), p. 19.

[42]M. H. Meynadier, E. Finkman, M. D. Sturge, J. M. Worlock, and M. C. Tamargo, Phys. Rev. B **35**, 2517 (1987).

[43]Y. R. Lee and A. K. Ramdas (unpublished); R. B. Bylsma, W. M. Becker, J. Kossut, U. Debska, and D. Yoder-Short, Phys. Rev. B **33**, 8207 (1986).

[44]G. C. Osbourn, J. Appl. Phys. **53**, 1586 (1982); J. Vac. Sci. Technol. B **1**, 379 (1983).

[45]R. B. Bylsma, R. Frohne, J. Kossut, W. M. Becker, L. A. Kolodziejski, and R. L. Gunshor, Mater. Res. Soc. Symp. Proc. **56**, 223 (1986).

[46]Y. Hefetz, J. Nakahara, A. V. Nurmikko, L. A. Kolodziejski, R. L. Gunshor, and S. Datta, Appl. Phys. Lett. **47**, 989 (1985).

[47]I. I. Novak, V. V. Baptizmanskii, and L. V. Zhoga, Opt. Spektrosk. **43**, 252 (1977) [Opt. Spectrosc. (USSR) **43**, 145 (1977)]; F. Cerdeira, A. Pinczuk, J. C. Bean, B. Batlogg, and B. A. Wilson, Appl. Phys. Lett. **45**, 1138 (1984).

[48]F. Cerdeira, C. J. Buchenauer, F. H. Pollak, and M. Cardona, Phys. Rev. B **5**, 580 (1972).

[49]S. Venugopalan and A. K. Ramdas, Phys. Rev. B **8**, 717 (1973).

[50]If we assume the elastic moduli for $Zn_{0.67}Mn_{0.33}Se$ to be the same as those for ZnSe, we get $(p-q)/2\omega_{LO}^2 \sim 0.86$ which is still significantly larger than that for ZnSe.

[51]R. R. Galazka, S. Nagata, and P. H. Keesom, Phys. Rev. B **22**, 3344 (1980); M. A. Novak, O. G. Symko, D. J. Zheng, and S. Oseroff, J. Appl. Phys. **57**, 3418 (1985).

[52]A. Petrou, D. L. Peterson, S. Venugopalan, R. R. Galazka, A. K. Ramdas, and S. Rodriguez, Phys. Rev. B **27**, 3471 (1983).

[53]R. L. Gunshor, L. A. Kolodziejski, N. Otsuka, B. P. Gu, D. Lee, Y. Hefetz, and A. V. Nurmikko (unpublished).

[54]D. U. Bartholomew, E.-K. Suh, S. Rodriguez, A. K. Ramdas, and R. L. Aggarwal, Solid State Commun. **62**, 235 (1987).

[55]J. Spalek, A. Lewicki, Z. Tarnawski, J. K. Furdyna, R. R. Galazka, and Z. Obuszko, Phys. Rev. B **33**, 3407 (1986); R. L. Aggarwal, S. N. Jasperson, P. Becla, and R. R. Galazka, *ibid.* **32**, 5132 (1985); B. E. Larson, K. C. Haas and R. L. Aggarwal, *ibid.* **33**, 1789 (1986).

[56]For details we refer to S. Rodriguez, A. Camacho, and L. Quiroga, Superlatt. Microstruct. (to be published).